ANNALS OF GEOPHYSICS, 61, 5, SE554, 2018; doi: 10.4401/ag-7638

"HYDRAULIC FRACTURE STUDIES OF RESERVOIRS WITH AN EMPHASIS ON PORE FRACTURE GEOMETRY STUDIES BY DEVELOPING FRACTURE AND MICROSEISMIC ESTIMATIONS"

Shanker Krishna[1,*], Hari Sreenivasan[1], Rajesh R. Nair[2,*]

(1) Petroleum Geomechanics Laboratory, Department of Ocean Engineering, Indian Institute of Technology Madras, Chennai, Tamil Nadu, India
(2) Petroleum Engineering, Petroleum Geomechanics Laboratory, Department of Ocean Engineering, Indian Institute of Technology Madras, Chennai, Tamil Nadu, India

Article history
Receveid **January 24, 2018**; accepted **June 19, 2018.**
Subject classification:
Computed Tomography; Fracture Propagation; Hydraulic Fracturing; Laser Doppler Vibrometer; Shear Wave Splitting.

ABSTRACT

Nondestructive measurements and evaluation has great significance in various domains of science, engineering and technology. The objective of this research is to investigate the anisotropic behavior in a sandstone sample from non-invasive tests using Laser Doppler Vibrometer coupled with Piezoelectric Transducer and to validate these results using a laboratory scale controlled hydraulic fracturing arrangement. High-resolution 3-component single-point seismograms were generated for the core sample using a combination of 1 MHz Piezoelectric Transducer as a source of elastic waves that travel within the reservoir rock sample and Laser Doppler Vibrometer as the receiver. Hilbert transforms of the 3-component data were calculated to obtain the complex signal. Shear wave splitting phenomenon due to anisotropy in rock was examined and the resultant S_H and S_V wave polarizations were measured. Elastic tensor for the core sample was subsequently determined from the velocity picks within the Hilbert energy envelope followed by the estimation of Thomsen's parameters. The hodogram analysis was performed to assess the process of shear wave splitting in the rock sample that detects the anisotropy of the medium and this, in turn, specifies the characteristics of weakness planes. Laboratory scale controlled hydraulic fracturing was performed to verify whether the fractures propagate along the anisotropic planes of weakness. Real-time fracture detection was carried out during this process and its propagation features were studied. The fractured core sample was imaged under the slice Computed Tomography scan machine to perceive the mode and propagation of fractures in the rock specimen.

1. INTRODUCTION

Hydraulic fracturing is one of the effective technology applied in the oil and gas industry and mining industry for reservoir stimulation. The reservoir is initially perforated and the fluid is injected into the target location at high pressure to create fractures. This results in permeable pathways in the formation which increases the reservoir permeability. Generally, tight formations are hydraulically fractured for improving the flow rates of oil and gas, thereby maintaining the well productivity. Hydraulic fracturing has been extensively studied but the ambiguity remains due to the heterogeneity of rocks and complex propagation of fractures.

The geometry of the fracture affects the propagation characteristics of the fracture, the flow direction and the stresses in rock. Fracture created in combination with the conductivity of the well determines the well productivity. The fracture orientations and extent depend on a variety of subsurface variables like faults, natural fractures, discontinuities, permeability variations, viscosity of fluid, heterogeneity, in-situ rock stresses, thermal stresses and rate of strain.

Several hydraulic fracture models have been devel-

oped over the past few decades such as PKN and KGD models which require assumptions like bi-wing symmetric planar fracture growth, elliptical fracture geometries, homogenous rock mechanical properties and simplified flow [Perkins and Kern, 1961; Nordgren, 1972, Geertsma and de Klerk, 1969]. Several laboratory scale studies [Johnson and Cleary, 1991; Warpinski, 1982; Behrmann and Elbel, 1991; Zhou et al., 2008; Weijers et al., 1994; Athavale and Miskimins, 2008] of hydraulic fracturing have been carried out through field cases [Warpinski, 1985; Jeffrey et al., 1995] which are essential for validation of computer models.

The process of hydraulic fracturing is highly complex due to heterogeneity in properties of material, structure of rock and stress state [Germanovich et al., [1997], as a result of which the prediction of the hydraulic fracture behavior is always difficult. Most of the hydraulic fracturing experimental studies were carried out on samples of rocks and sediments [Hanson et al., 1982; Medlin and Masse, 1984]. Studies on non-linear effects in propagation of fracture in cement paste blocks [de Pater et al., 1994; Groenenboom and van Dam, 2000] and on non-planar fracture geometries, as a result of initiation and propagation of fracture, in gypsum cement blocks [Abass et al., 1996] were carried out.

During hydraulic fracture studies in materials that are opaque in nature there is always a difficulty in observing, determining and measuring the fractures formed. The sample is cut to study the induced fracture geometry after carrying out the test [de Pater et al., 1994; Abass et al., 1996], to measure fracture profile and radius using acoustics [de Pater et al., 1994; Groenenboom and van Dam, 2000]. Some of the commonly used materials for hydraulic fracturing studies are polymethylmethacrylate (acrylic) [Rummel, 1987; Cooke and Pollard, 1996; Germanovich and Dyskin, 2000] and polycarbonate [Rittel, 2000]. Experiments were conducted to study the fracture formation in glass [Sommer, 1969; Germanovich et al.,1994], crack growth in polyester resin [Sahouryeh et al., 2002] and crack growth in a gelatin material [Hubbert and Willis, 1957; Takada, 1990]. Laboratory study was performed to evaluate this critical state geometry by injection of epoxy into acrylic and granite [Frash et al.].

Several methods have been used for monitoring and measuring the hydraulic fracture geometries which include acoustic emissions, well-logs, impression of packers, displacement measurement, analysis of tilt data using tilt meter [Lecampion and Peirce 2007] and using cores. Several techniques have been adopted to have better control over the orientation of fractures. Pressure for fracture initiation is reduced by creation of a starter fracture. Germanovich et al., [1999] made circular turns using a bent which was used to generate a starter fracture in the specimen. Bunger et al., [2004] generated a starter fracture by placing and striking a rod in the tube of injection.

Segmentation and the branching of hydraulic fracture are widely seen in nature [Roering, 1968; Pollard et al., 1982; Pollard and Aydin, 1988; Rubin, 1995; Abelson and Agnon, 1997]. While conducting laboratory tests in homogenous materials, the hydraulic fracture front splitting is observed [Hubbert and Willis, 1957; Knauss,1970; Hallam and Last, 1991; Abass et al., 1996; Bakala, 1997]. In an experiment performed in the laboratory on hydraulic fracturing, segmentation was observed by Hubbert and Willis [1957]. Blocks made of gypsum cement were tested in a tri-axial loading vessel which resulted in observation of multiple segmentation of fractures [Abass et al., 1996]. In general, the primary causes for segmentation and branching of fractures are heterogeneity in stress and material properties [Germanovich et al., 1997]. In geomaterials, one of the fundamental reason for segmentation of fracture is stress heterogeneity [Delaney and Pollard, 1981; Cooke and Pollard, 1996; Germanovich et al., 1997]. Typically, in proximity to a fracture front, deformation can happen in three modes [Kanninen and Popelar, 1985]. The type of loading can be in mode I, mode II or mode III or a typical combination of these. Fracture growth under mixed mode is also studied extensively.

Acoustic and seismic studies have always played an important role in reservoir characterization. Calibration in acoustic and seismic studies of reservoir rocks is done by means of laboratory measurements for the estimation of elastic anisotropy. “Time of flight” is one of the common methods by which the rock sample anisotropy is measured. The rock sample anisotropy is measured by determining the wave velocities. Stiffness tensor, which is density scaled, is determined by measuring the velocities of compressive wave and shear wave along different directions with respect to the axes of the samples under test.

The travel times of waves, produced and logged by a piezoelectric transducer, is used for determining the wave velocities [Pros and Babuska, 1967; Jech, 1991; Rasolofosaon and Zinszner, 2002]. Piezoelectric transducers are used in ultrasonics as sources and receivers, though, experiments have some uncertainties linked to it. Shear wave arrival time determination is an uncertainty and also the fact that whether the velocity measured is phase or group. When the wave source size is smaller as compared to the sample used for measurement, the velocity measured is group velocity. If the

source size is in proportion to the sample size, the velocity of propagation of wave in the perpendicular direction is the phase velocity. The size of the receivers in seismic measurements is much smaller when compared to the recorded waves' wavelength. Estimation of polarization is simplified and also the determination of the type of wave. In-situ estimation of anisotropy by using polarization of waves and their velocities is one of the firmest methods [Dewangan and Grechka, 2003] and such techniques require receivers that are smaller when compared to the wavelength.

Laser Interferometry is one of the important techniques for the determination of arrivals of acoustics waves. Source of elastic waves is the pulsed laser and the receiver is a laser interferometer [Dainty, 1975; Ennos, 1978; Monchalin, 1986; Monchalin et al., 1989; Scruby and Drain,1990; Jacquot and Fournier, 2000)]. Elastic properties of materials that are isotropic in nature can be determined by means of laser interferometry [Aussel and Monchalin, 1989; Pouet and Rasolofosaon, 1993] which has also been used for materials with anisotropic nature [Guilbaud and Audoin, 1999; Ogi et al., 2003], particularly, [Pouet and Rasolofosaon, 1990; Martin et al., 1994, and Rasolofosaon et al., 1994] for determining quasi S-wave polarizations, for detection of shear wave [Nishizawa et al., 1997]. The method proposed by Nishizawa et al., in 1997, used wave induced propagation measurement of a smaller area on sample surface. For the separation of P and S waves, measurements are carried out in two separate directions and the displacement projections are determined on surfaces parallel and perpendicular to it. The displacements in tangential and normal directions can be determined by laser peckle type interferometry [Bayon and Rasolofosaon, 1996].

Fukushima et al., in 2003, used laser doppler interferometer for investigating the shear wave polarization in rock samples. Major advantage of laser doppler interferometry is that it enables recording of complete particle velocity and also the measurement area is smaller when compared to the wave length.

In this paper, the anisotropic behavior of a sandstone sample is studied by integrating the outcomes of Laser Doppler Vibrometer coupled with Piezoelectric Transducer and the laboratory scale hydraulic fracturing arrangement. Shear wave splitting due to anisotropy is analyzed and elastic tensor of the core sample is calculated. Lab scale controlled hydraulic fracturing is then performed to verify whether the fracture propagates along the anisotropic plane of weakness. The Computed Tomography image of the fracture is obtained to study its characteristics and the type of loading in clarity. A real-time pressure-time plot is generated that monitors the pressure at which the core sample is fractured. Fracture orientations predicted by the non-invasive studies using Laser Doppler Vibrometer coupled with Piezoelectric Transducer and the results of hydraulic fractur-

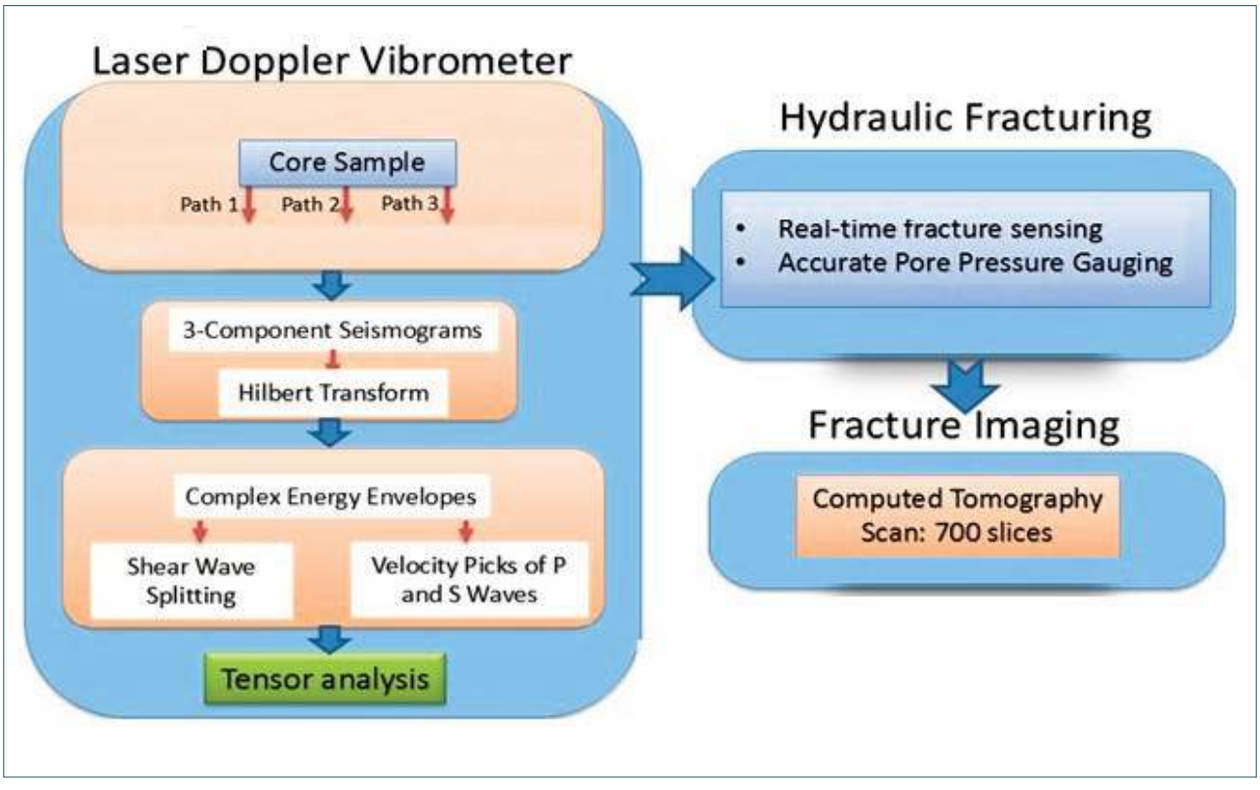

FIGURE 1. Project Workflow

ing are compared by means of a stereonet plot.

The presented workflow of the research is shown in Figure 1. High resolution 3-component single-point seismograms in the core sample is generated using a combination of Piezoelectric Transducer and Laser Doppler Vibrometer. We use a Laser Doppler Vibrometer as a receiver and a 1 MHz Piezoelectric Transducer as a source of disturbance for this purpose.

Hilbert transform is computed upon the 3-component signal to obtain the complex signal. Shear wave splitting due to anisotropy in rock is checked for and the resulting S_H and S_V wave polarizations are measured. Elastic tensor of the core sample is then calculated using the velocity picks from the Hilbert energy envelope.

Laboratory scale controlled hydraulic fracturing is then performed to verify whether the fracture propagates along the anisotropic plane of weakness. After fracturing, the core sample is then imaged under Computed Tomography using a Siemens 700 Slice CT scan machine to see the rock fracture propagation and type of loading in clarity.

2. LASER DOPPLER VIBROMETER

In this experiment, Melectro V100 Laser Interferometer (Figure 2) recorded the motion at a point on the rock surface. Ritec RPR-4000 Pulser Receiver is used to give high quality high frequency pulse to the Piezoelectric Transducer which is attached below the sample to generate the source impulse. We particularly chose 160 kHz frequency input to the piezoelectric transducer with 12.6 us pulse length and 6.3 us pulse wavelength. The piezoelectric transducer used were of either 1 MHz or 2 MHz resonant frequency and with an average diameter of 14mm. A Pico scope is used to view the high-resolution signal output from the Laser Doppler Vibrometer.

FIGURE 2. Setup of Laser Doppler Vibrometer.

As a wave source, the piezoelectric transducer is glued to the lower-end of the sample such that the polarization of the source is at an orientation of 45° to X and Y axes. The piezoelectric transducer, in such a position, results in generation of shear waves in vertical and horizontal directions along with the P wave. A reflective tape of 3M make was glued on to the surface of the core sample which is diametrically opposite to the surface where the transducer was placed. The tape contains micro-beads made of glass which makes light to be reflected backward [Lebedev et al., 2011].

2.1 CO-ORDINATE TRANSFORMATION

Particle displacements and velocity spatial components are to be determined in minimum of three directions and such that the 3D space is covered (Figure 3). Determination of polarization is by measurement of linearly independent three components of displacement or particle velocity. P and S wave arrival times and the corresponding polarizations that imply the direction of particle motion are determined from these measurements.

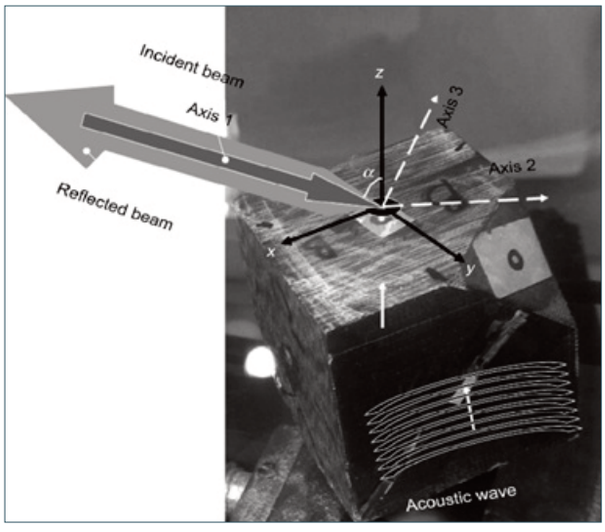

FIGURE 3. Displacement measurement schematic of the three-components [Lebedev et al., 2011].

2.2 VELOCITY PICKING

Hilbert transform is applied to the obtained 3-component data after co-ordinate system transformation to get a complex envelope with phase values at every point and the energy envelopes. These are very useful to detect the incoming energy packet, whether it may be from P-wave, S_H wave or S_V wave in a 3-component seismogram.

Hilbert energy envelope with phase information aids in the manual P-wave and S-wave picking, thus providing the respective velocities. The MATLAB open source code of SEIS_PICK is used for this purpose. It provides a frequency spectrum analysis to get the fre-

quency ranges of the signal and the noise which then can be separated using a bandpass filter, as shown in Figure 9 [James, 2012].

The X and Y components are represented in red and green, respectively and the vertical components in blue. The energy envelope is depicted in grey. Also, P wave start and end is depicted in black and blue and the S wave start and end in red and green, respectively. P wave azimuths, where hodogram analysis is carried out, are also represented.

2.3 HODOGRAM ANALYSIS

Principle component analysis is performed on windows of P and S wave through which the hodogram analysis is obtained and this gives a measure of the particle motion. The seismic event azimuth is inferred from the P wave particle motion. For multiple azimuths, MATLAB package of circular statistics is used by SEIS_PICK for computing the average azimuth at 95% confidence limits (Figure 10) [James, 2012].

The angle between particle motions of P and S wave and also the polarization of S wave is calculated. The window of traces is replaced by the hodogram analysis with the output of particle motion data and also the list of polarization angles.

In borehole seismology, hodograms are generally used for determining the shear wave splitting and wave arrival directions.

Hodogram analysis provides information about the 3-D particle motion which is created due to the impulsive disturbance produced by the Piezoelectric Transducer and measured by the Laser Doppler Vibrometer on the surface of the sample.

2.4 SPECTRAL ANALYSIS

For the selected traces SEIS_PICK also provides a spectral analysis platform. The pre-event noise, comprising of P wave and S wave windows and frequency content, is computed by MATLAB fft function. The platform provides each component of the spectra separately. The P wave, S wave and pre-event noise is depicted in red, green and blue respectively (Figure 11) [James, 2012].

2.5 ELASTIC STIFFNESS TENSOR

Material density and stiffness tensor determines the elastic wave propagation in a rock sample. The wave polarization and phase velocity are connected to stiffness tensor by Christoffel equations [Cerveny, 2005]

$$c_{ijkl}p_jA_kp_l=\rho A_i \tag{1}$$

where c, p, A, ρ are the stiffness tensor, phase slowness, polarization and density.

Polarizations are mutually orthogonal during the wave propagation by three modes in an anisotropic media which are quasi-longitudinal, quasi-shear and pure shear. Once velocities are determined, the elastic stiffness tensor is obtained by Christoffel equations [Liao et al., 1997; Lo et al., 1986; Hornby 1998; Sarout 2007, Oliver et al., 2016]:

$$\mathbf{c_{11}}=\rho\mathbf{v}^2_{p(0°)},\ \mathbf{c_{33}}=\rho\mathbf{v}^2_{p(90°)},\ \mathbf{c_{44}}=\rho\mathbf{v}^2_{s(0°)},\ \mathbf{c_{66}}=\rho\mathbf{v}^2_{p(90°)} \tag{2}$$

$$c_{13}=-c_{44}+\left[\frac{1}{\sin^2 2\theta}\ (2\rho VP_\theta^2-2c_{11}\ \sin^2\ \theta+c_{44}(\sin^2\theta\ -\ \cos^2\text{-}1)\ X\right.$$
$$\left.(2\rho Vp_\theta^2\ \text{-}2c_{33}\cos^2\theta+c_{44}(\cos^2\theta\ \text{-}\ \sin^2\theta\ \text{-}\ 1)\right]^{\frac{1}{2}} \tag{3}$$

The resulting elastic stiffness matrix of transverse anisotropy [Thomsen, 1986] is given by

$$C_{\alpha\beta}=\begin{pmatrix} c_{11} & c_{11}-2c_{66} & c_{13} & 0 & 0 & 0\\ c_{11}-2c_{66} & c_{11} & c_{13} & 0 & 0 & 0\\ c_{13} & c_{13} & c_{33} & 0 & 0 & 0\\ 0 & 0 & 0 & c_{44} & 0 & 0\\ 0 & 0 & 0 & 0 & c_{44} & 0\\ 0 & 0 & 0 & 0 & 0 & c_{66} \end{pmatrix} \tag{4}$$

and the P wave and S wave velocities parallel to the symmetry axis are, respectively, given by

$$\alpha=\left(\frac{c_{33}}{\rho}\right)^{\frac{1}{2}}$$
$$\beta=\left(\frac{c_{44}}{\rho}\right)^{\frac{1}{2}} \tag{5}$$

2.6 THOMSEN'S PARAMETERS

For characterization of transversely isotropic materials [Thomsen, 1986], the elastic moduli parameters, denoted by ε, δ and γ, are determined and they are dimensionless.

$$\varepsilon=\left(\frac{c_{11}-c_{33}}{2c_{33}}\right)$$
$$\delta=\frac{(c_{13}+c_{44})^2-(c_{33}+c_{44})^2}{2c_{33}(c_{133}+c_{44})^2} \tag{6}$$
$$\gamma=\frac{c_{66}-c_{44}}{2c_{44}}$$

These results, when combined with P and S wave velocities, can be used to characterize propagation of wave through an anisotropic medium.

3. LABORATORY SCALE HYDRAULIC FRACTURING SETUP

Hydraulic fracturing experiments are carried out by pumping a fluid into a sample at a high pressure. The laboratory scale hydraulic fracturing setup is shown in Figure 4. The process of hydraulic fracturing requires specific instruments and accessories like tanks for storing fluids, pumping devices, containers for transporting proppants and other auxiliary equipment's like valves, flexible hoses, inlet outlet manifolds. Also, the setup requires appropriate controlling and monitoring equipments to have details on the variables.

predictable flow, control of pressure and precision. In order to have safety at high pressure and to prevent leaks, fittings are provided. The materials wetted can be used with liquids which are organic, corrosive, of high temperature and also slurries. The functions of control system components are as stated, Pressure transducer – pressure read out as an analog signal; PLC controller – PID controller for the set pressure; Variable Frequency Converter – to control the hydraulic pump; and Human machine interface – pressure read out, pressure programming and data logging. The system is provided with an emergency stop button and also is covered with toughened acrylic door for visibility and safety.

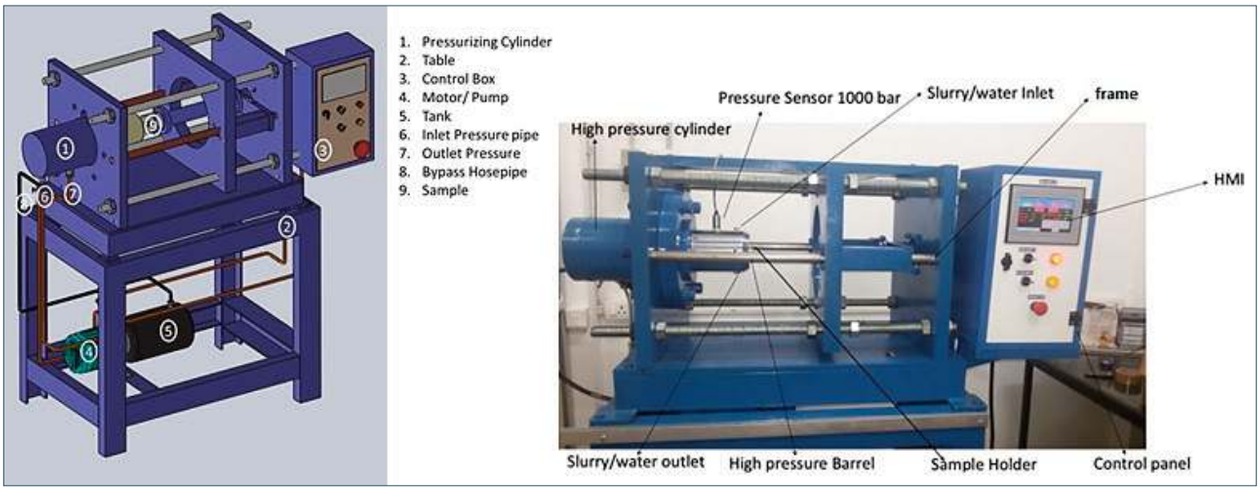

FIGURE 4. Laboratory Scale Hydraulic fracturing setup.

3.1 GENERAL SPECIFICATIONS

The equipment with a capacity of 1000 bar and a least count of 1 bar has a four-digital RS 485 communication display. Water, sand with water mixer, gel with water mixer and gas (methane) can be used as pressuring items.

The connection of sample is done either with a connector or hydraulically. Total number of cylinders for the pressure system are two with one at the top and the other one at the bottom. The system body is made from H type MS steel construction.

The high-pressure pumps are driven by motor and are of positive displacement type, custom made for catalyst injection and other fluids in highly pressurized systems. The high-pressure mechanism is achieved through a hydraulic system which is a geared hydraulic pump. The hydraulic motor is rated 2 HP/ 415V AC and 3.5 LPM with a maximum pressure of 1000 bar. Pressure transducer has a range of 0-1000 bar. Drive train, which is of single ratio and auto lubricating gears with longer life and lesser maintenance, is used. For high pressure applications, like deep well core analysis, the pump is suitable as it has a

3.2 EXPERIMENTAL PROCEDURE

The core sample used for study is sandstone and is cylindrical in shape. Along the central axis of sample, a smaller diameter hole is drilled. In order to reduce the boundary effects, the drill hole diameter is minimized. A casing like connecter is tapped into the sample surface and the top surface of the sample is connected to the pressure outlet of the fracturing setup. For initiation and propagation of fractures, a fluid is injected into the sample for fracturing through the hole drilled and the casing.

Water is used as the fracturing liquid for the experiment performed in the lab.

The casing is drilled with a minor interference to the cylindrical sample and is tapped slowly into the hole drilled. The process is done by tapping with a hammer [Bunger et al., 2004; Hull, 1994] or a loading machine.

The loading is static and can be controlled such that starter fractures are formed which are orthogonal to the drill hole and is also circular in shape.

3.3 FRACTURE SIZE

Size of fracture is controlled by changing the volume of fluid that is injected in between the fracture and the pump (Figure 5). For a stiff pump, that is ideal, there is compression of fracturing fluid occupied and accumulation of strain energy. Formation of fracture occurs at peak pressure. As there is a drop in the pressure, the propagation of fracture ceases once this energy is released. Based on the model the estimation of fracture size can be done.

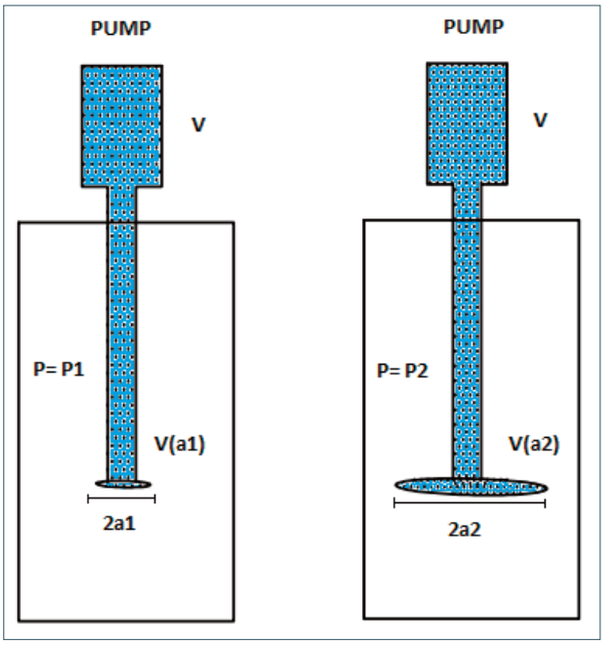

FIGURE 5. Initial and final instances of fracture propagation. [Wu et al., 2007].

Consider the fracture propagation in the initial and final instances which commences from a small starter fracture. The starter fracture grows as the pressure of fluid reaches its peak, p1 and the propagation stops at a value p2 due to pressure drop. As the fracture growth period is very short, the fluid additionally injected by the pump during this time is ignored. The associated assumption is valid for a low rate of injection and high stiffness pump, i.e. the mass of fluid in the fracture and tubing is a constant during the propagation of fracture. As a result, pump design is not a priority and a drill hole with metal casing is considered [Wu et al., 2007].

3.4 FRACTURE PROPAGATION AND SEGMENTATION

Typically, in the proximity of a fracture front deformation can happen in three modes. In mode I, displacements of fracture surface are perpendicular to the plane of fracture (Figure 6a). In mode II, displacements of fracture surface are orthogonal to the fracture front and also in fracture plane. (Figure 6b). Mode III is formed by fracture surfaces that are displaced due to shear and are parallel to the fracture front (Figure 6c) [Kanninen and Popelar, 1985].

The loading of fracture is possible under pure modes (Figure 7a) individually or a combination of them. If loaded under combination, then it is termed as loading under mixed mode. Out of plane propagation is generally produced in the case of mixed mode fractures [Pollard and Aydin, 1988]. Mixed-mode I+II is termed as in-plane shear which, when formed, results in fractures in curved shape with sharp twists (Figure 7b). Mixed-mode I+III is termed as out-of-plane shear as a result of which fracture fronts are segmented (Figure 7c).

Mechanism of relieving in mode I is fracture growth, mode II by changing direction of fracture propagation and mode III by segmentation.

4. RESULTS AND DISCUSSIONS

The core samples provided by Oil India Limited were used to carry out anisotropic characterization studies with Laser Doppler Vibrometer coupled with Piezoelectric Transducer. In this core sample, the bedding plane discontinuity (weaker planes in a hexagonal system) was detected and the elastic tensor was calculated.

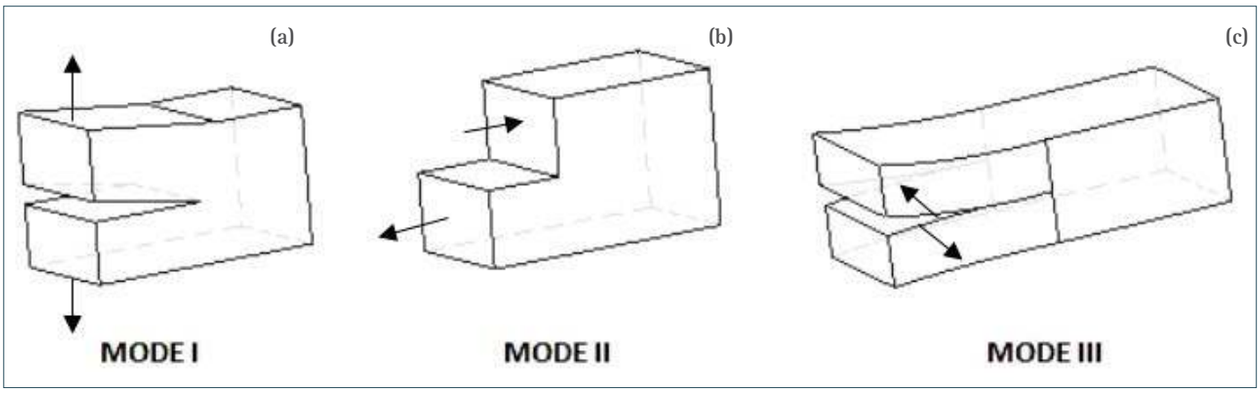

FIGURE 6. Three modes of fractures: (a) mode I, (b) mode II, and (c) mode III.

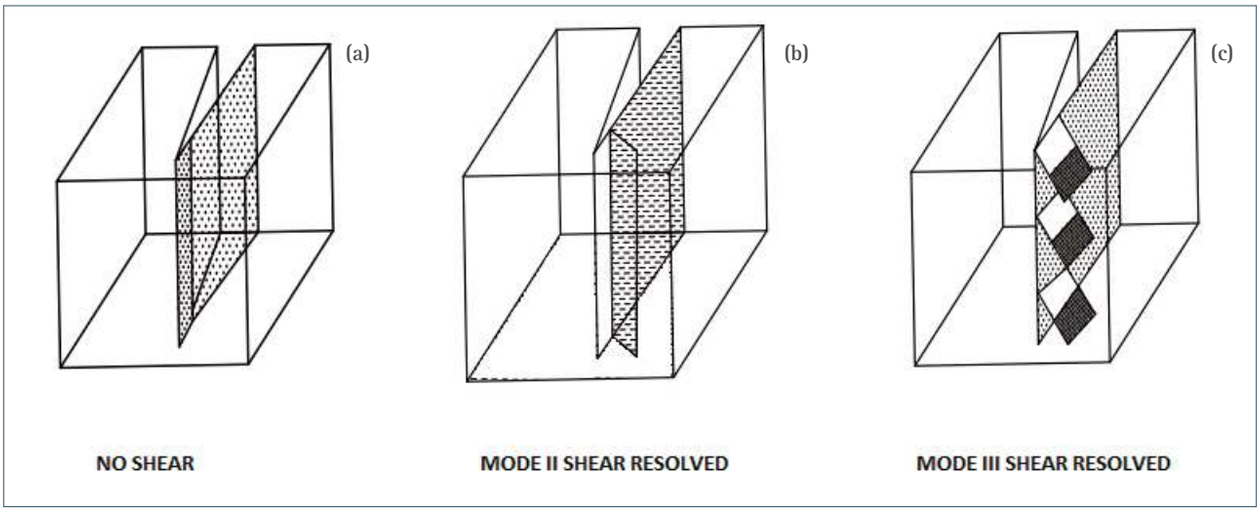

FIGURE 7. Fracture propagation path illustration: (a) pure mode I, (b) mixed-mode I+II, and (c) mixed-mode I+III.

4.1 CORE SAMPLE

Oil sandstone specimen from well NHK#332 in Tipam 60 reservoir (Figure 8) is of 11cm length. The specimen belongs to a depth of 2750 m and shows visible fine near-horizontal bedding laminations.

For this purpose, high-resolution 3-component single-point seismograms were generated for vertical orientation (0 degree), diagonal orientation (45 degrees) and horizontal orientation (90 degrees) with respect to the axis of the core sample.

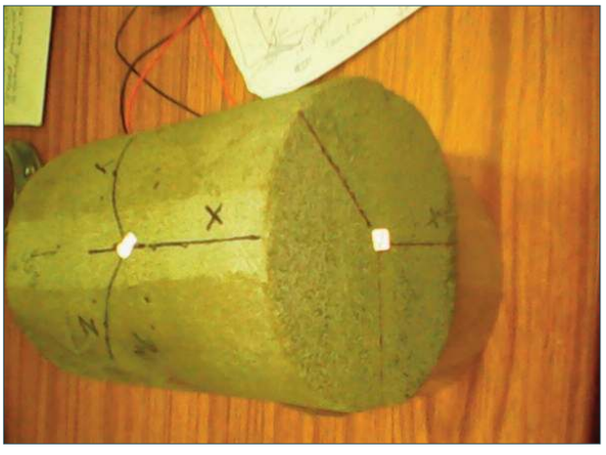

FIGURE 8. Sandstone Core sample.

4.2 THREE COMPONENT SEISMOGRAMS

The 3-component seismogram in the vertical, diagonal and horizontal orientations are shown in Figure 9. The input pulse to the piezoelectric transducer was given at t = 50 us. The velocity picks were done considering the relative polarizations of P-wave, SH wave and SV wave.

4.3 HODOGRAM ANALYSIS

The hodogram analysis for the velocity picks is carried out and the azimuths of the P wave and S wave polarizations are obtained as in Figure 10.

The hodogram graphically depicts the particle motion with the P wave and S wave as shown in the plots (Figure 10) where the P wave trace is represented in red and S wave trace in green.

4.4 SPECTRAL ANALYSIS

The spectrum of pre-event noise is shown in blue color, P wave in red and S wave in green, as shown in Figure 11. The spectral analysis enables to view the frequency content of each phase and the pre-event noise.

4.5 SHEAR WAVE SPLITTING

Then shear wave splitting was checked for and the polarizations of the horizontal and vertical shear waves (SH wave and SV wave) were measured. Figure 12 illustrates the shear wave splitting detected in the given sample for the ray travel path and also demarcates the SH wave and SV wave polarizations.

4.6 STEREONET PLOT

Since the vertical shear wave is polarized along a plane perpendicular to the plane of hexagonal anisotropy, we use them to delineate the probable weak plane (bedding plane), by plotting the vertical shear wave polarizations on a Schmidt Equal Area Net. We sometimes also use cross products of horizontal shear waves (e.g. SH (0) X SH (45)) to get the vector perpendicular to the bedding planes (Figure 13). Since, there are three such cross-product combinations, we use them as well wherever we were confident about their polarizations. The following figure shows a stere-

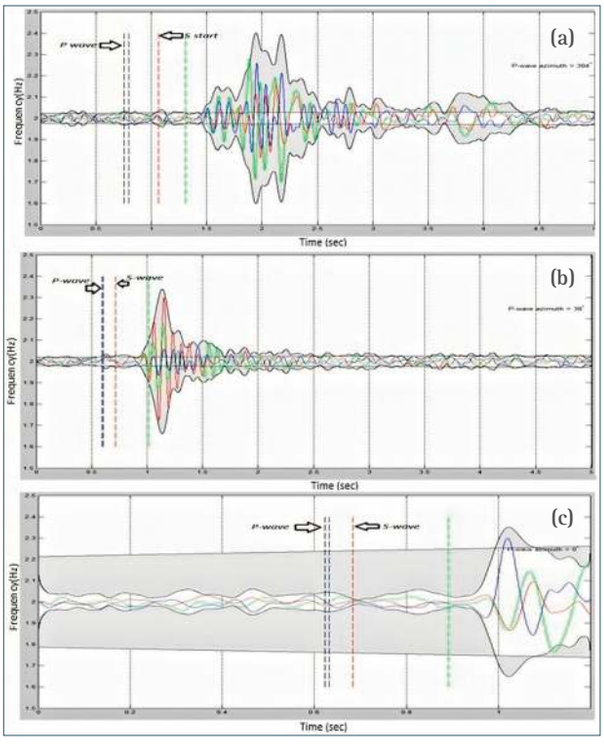

FIGURE 9. 3 Component seismograms in (a) Vertical, (b) Diagonal and (c) Horizontal orientations in which X and Y components represented by red and green and vertical components by blue. The energy envelope is depicted in grey. P wave start and end is depicted by black and blue and also S wave start and end by red and green respectively. P wave azimuths are also represented where hodogram analysis is carried out.

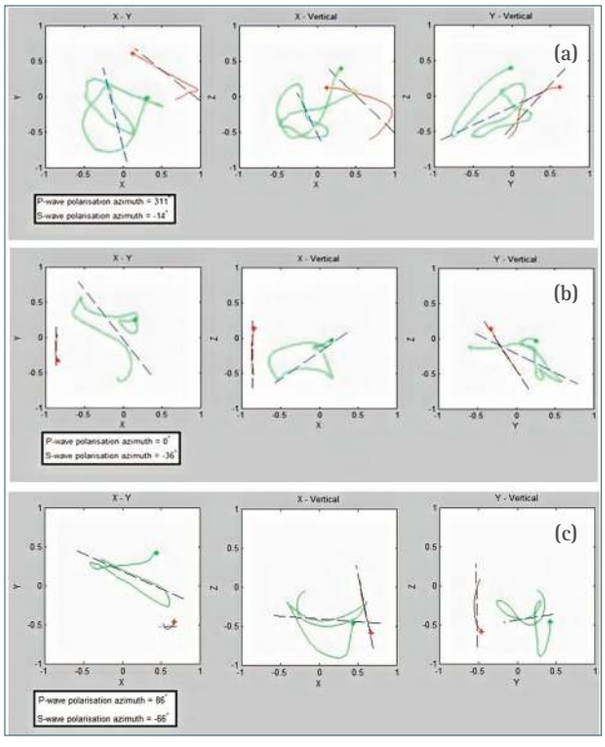

FIGURE 10. Hodogram for particle motion with P-wave represented in red and S wave in green in (a) Vertical, (b) Diagonal and (c) Horizontal orientations.

onet plot of the hence obtained probable poles to the bedding planes. The elastic tensor obtained is shown below in Table 1.

The Thomsen's parameters are determined as δ=-0.0902739, ε=0.17857264, γ=0.50671379 and the P-wave velocity and S-wave velocity as α=3147 m/s, β=1507 m/s, respectively.

The rock sample is hydraulically fractured in the laboratory scale hydraulic fracturing set up. The pressure time graph of the fracturing process is shown in Figure 14, where the fracture pressure is 8 bars. Figures 15 and 16 show the Computed Tomography (CT scans) of core sample after hydraulic fracturing.

This figure is an overall inside-out view of sample showing the horizontal fracture at a depth of 42.1 mm from the top.

In Figure 16, to the right, a slice view in the same orientation is shown depicting the fracture propagation path. Magnified view of Figure 15, marked in a yellow box showing a maximum fracture opening of 2.1 mm, is shown in Figure 16. Figure 17 shows the hair lines in curved shape on the core sample where the fractures are formed indicating the type of loading to be mixed mode showing segmentation.

Elastic Stiffness Tensor (GPa)					
36.4739805	9.37618	11.7942	0	0	0
9.37618328	36.474	11.7942	0	0	0
11.7942217	11.7942	26.2585	0	0	0
0	0	0	5.96819	0	0
0	0	0	0	5.96819	0
0	0	0	0	0	13.5489

TABLE 1. Anisotropy elastic tensor.

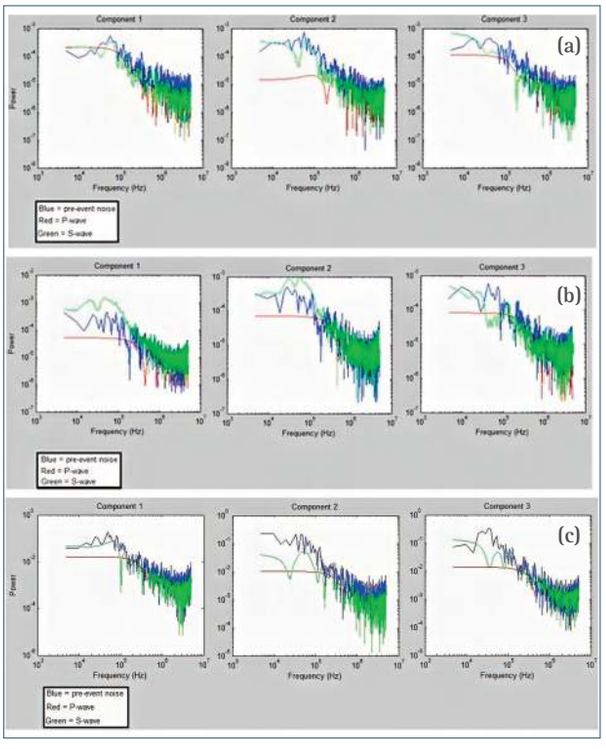

FIGURE 11. Spectral analysis platform provides each component of the spectra separately. P wave, S wave and pre-event noise is depicted in red, green and blue, respectively, for (a) Vertical, (b) Diagonal and (c) Horizontal orientations

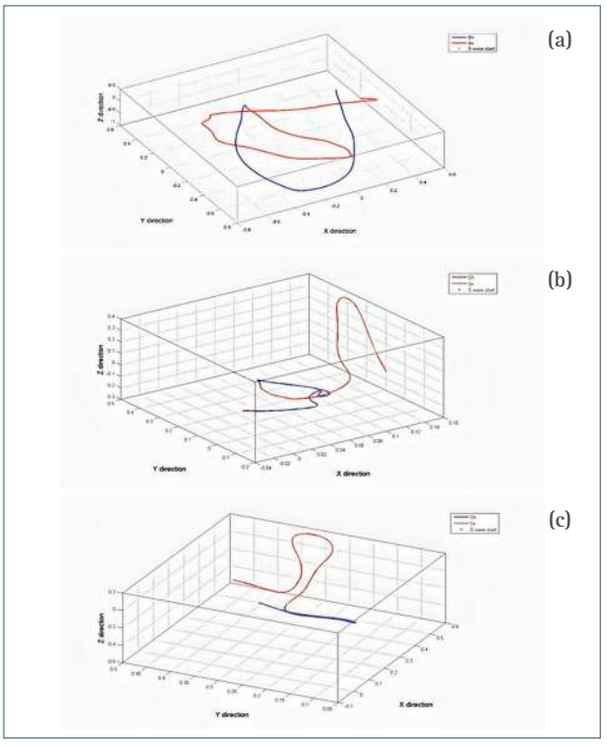

FIGURE 12. Shear wave splitting for (a) Vertical, (b) Diagonal and (c) Horizontal orientations

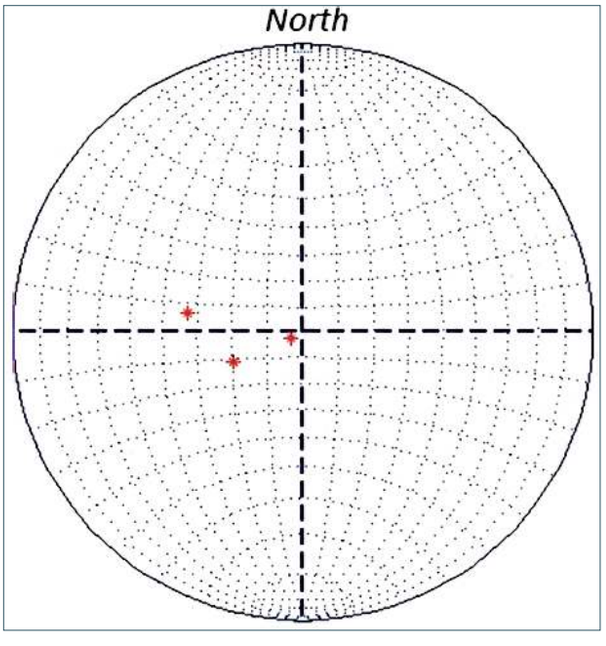

FIGURE 13. Stereonet plot.

5. CONCLUSIONS

The study explains the usage of non-invasive laboratory scale seismic investigations carried out on the sandstone specimen in characterizing its elastic properties and anisotropy.

This investigation determines the orientation of anisotropic plane of weakness based on the tests using Laser Doppler Vibrometer coupled with Piezoelectric Transducer.

The hodogram analysis was performed in each case to evaluate the process of shear wave splitting, an indicator of anisotropy in the subsurface geological structures, and the orientation of anisotropic plane of weakness was obtained from the stereonet plot.

The Thomsen's parameters δ, ε and γ determined for the specimen project the weak anisotropy of the medium as explained in Thomsen [1986].

The tested sandstone core sample was subjected to fracturing using the laboratory scale controlled hydraulic fracturing setup.

The orientation of fracture, as seen in the CT scan image of the fractured sample, corresponds with that of the anisotropic plane of weakness in the stereonet plot. The magnified view of the fracture in Computed Tomography indicates segregation and mixed mode loading is observed.

Such experiments focusing on the process of shear wave splitting can be used to evaluate the anisotropy in oriented hydraulic fracturing and other rock characterization studies.

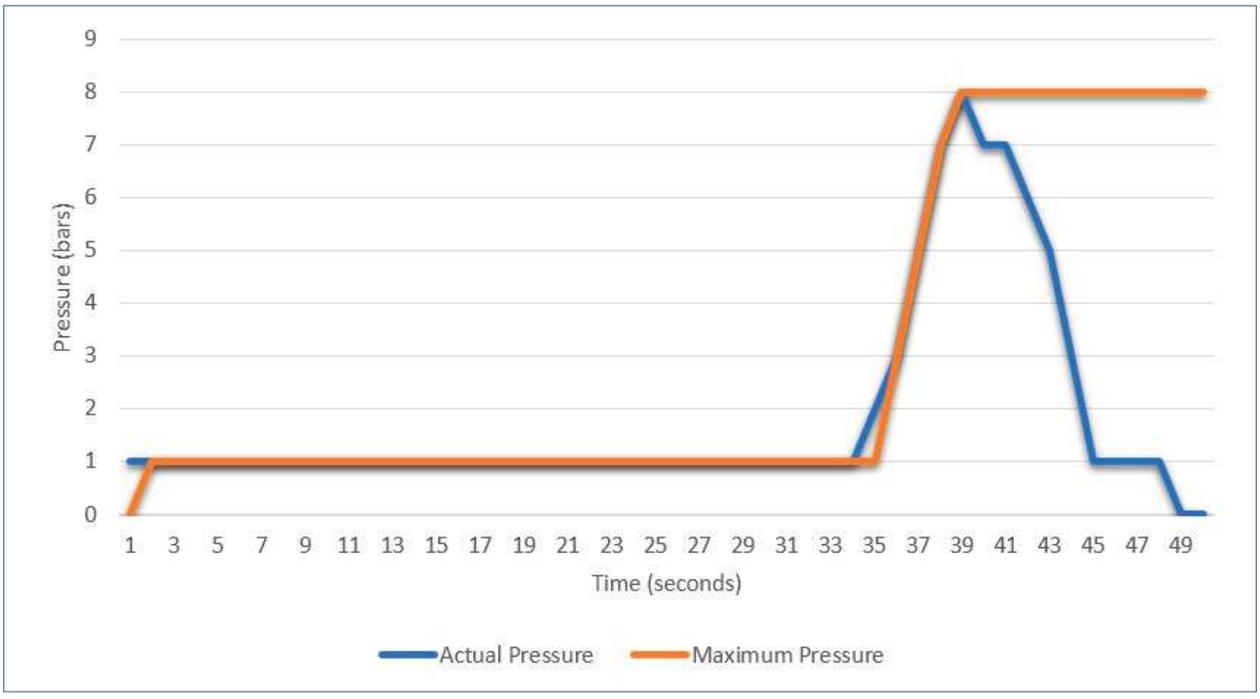

FIGURE 14. Real-time Pressure-Time graph during fracturing.

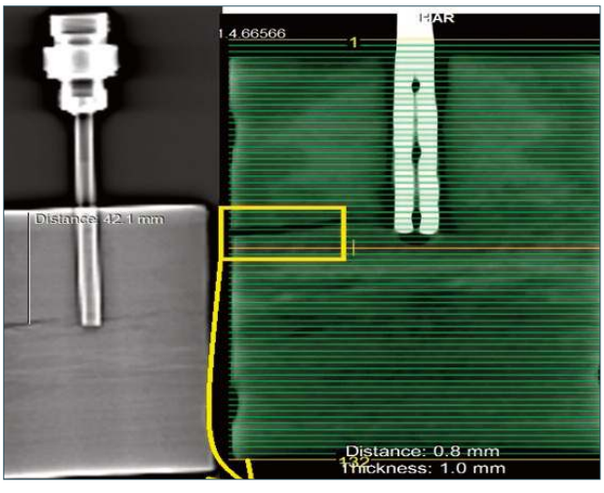

FIGURE 15. Fracture imaging using Computed Tomography.

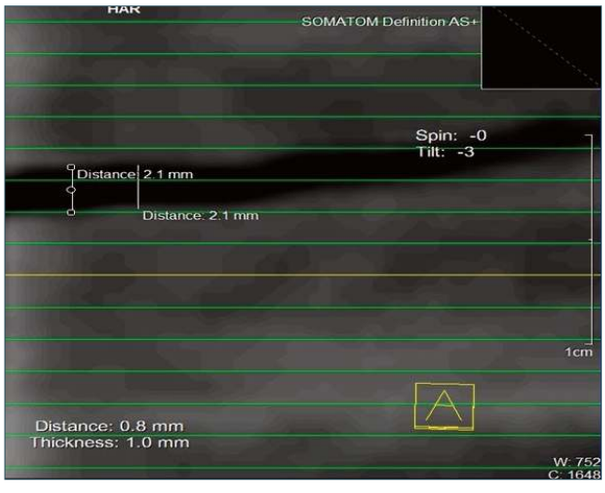

FIGURE 16. Zoom in view of fracture using Computed Tomography (zone marking yellow box).

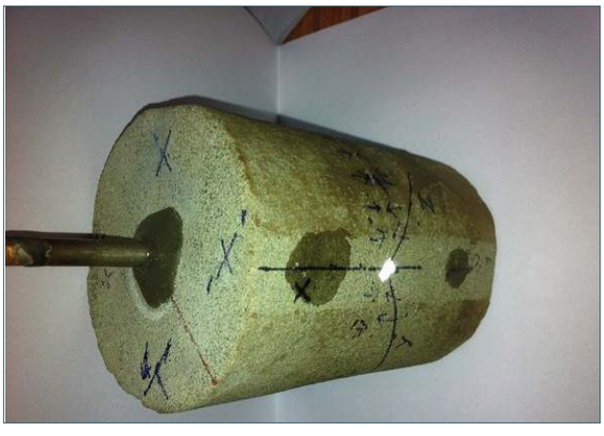

FIGURE 17. Fracture orientation as seen on sample surface.

Acknowledgements. The authors would like to thank Oil India Limited for the core samples and the funding for establishing the hydraulic fracturing facility. The authors would also like to thank the reviewers for their time and valuable suggestions.

REFERENCES

Abass, H. H., Hedayati, S., and Meadows, D. L. (1996). Nonplanar fracture propagation from a horizontal wellbore: experimental study. SPE Production and Facilities, 11(03), 133-137.

Abelson, M., and Agnon, A. (1997). Mechanics of oblique spreading and ridge segmentation. Earth

and Planetary Science Letters, 148(3-4), 405-421.

Athavale, A. S., and Miskimins, J. L. (2008, January). Laboratory hydraulic fracturing tests on small homogeneous and laminated blocks. In The 42nd US Rock Mechanics Symposium (USRMS). American Rock Mechanics Association.

Aussel, J. D., and Monchalin, J. P. (1989). Precision laser-ultrasonic velocity measurement and elastic constant determination. Ultrasonics, 27(3), 165-177.

Bakala, M. (1997). Fracture propagation in sediment-like materials (Doctoral dissertation, University of Oklahoma).

Bayón, A., and Rasolofosaon, P. N. J. (1996). Three component recording of ultrasonic transient vibration by optical heterodyne interferometry. The Journal of the Acoustical Society of America, 99(2), 954-961.

Behrmann, L. A., and Elbel, J. L. (1991). Effect of perforations on fracture initiation. Journal of Petroleum Technology, 43(05), 608-615.

Bunger, A. P., Jeffrey, R. G., and Detournay, E. (2004, January). Toughness-dominated near-surface hydraulic fracture experiments. In Gulf Rocks 2004, the 6th North America Rock Mechanics Symposium (NARMS). American Rock Mechanics Association.

Cerveny, V. (2005). Seismic ray theory. Cambridge university press.

Cooke, M. L., and Pollard, D. D. (1996). Fracture propagation paths under mixed mode loading within rectangular blocks of polymethyl methacrylate. Journal of Geophysical Research: Solid Earth, 101(B2), 3387-3400.

Dainty, J. C. (1975). Laser speckle and related phenomena: Springer Verlag.

Delaney, P. T., and Pollard, D. D. (1981). Deformation of host rocks and flow of magma during growth of minette dikes and breccia-bearing intrusions near Ship Rock, New Mexico (No. 1202). USGPO.

Dellinger, J., and Vernik, L. (1994). Do traveltimes in pulse-transmission experiments yield anisotropic group or phase velocities?. Geophysics, 59(11), 1774-1779.

De Pater, C. J., Weijers, L., Savic, M., Wolf, K. H. A. A., Van den Hoek, P. J., and Barr, D. T. (1994). Experimental study of nonlinear effects in hydraulic fracture propagation (includes associated papers 29225 and 29687). SPE Production and Facilities, 9(04), 239-246.

Dewangan, P., and Grechka, V. (2003). Inversion of multicomponent, multiazimuth, walkaway VSP data for the stiffness tensor. Geophysics, 68(3), 1022-1031.

Ennos, A. E. (1978). IV Speckle Interferometry. Progress in Optics, 16, 233-288.

Frash, L. P., Hood, J., Gutierrez, M., Huang, H., and Mattson, E. (2014, August). Laboratory measurement of critical state hydraulic fracture geometry. In 48th US Rock Mechanics/Geomechanics Symposium. American Rock Mechanics Association.

Fukushima, Y., Nishizawa, O., Sato, H., and Ohtake, M. (2003). Laboratory study on scattering characteristics of shear waves in rock samples. Bulletin of the Seismological Society of America, 93(1), 253-263.

Geertsma, J., and De Klerk, F. (1969). A rapid method of predicting width and extent of hydraulically induced fractures. Journal of Petroleum Technology, 21(12), 1-571.

Germanovich, L. N., Astakhov, D. K., Mayerhofer, M. J., Shlyapobersky, J., and Ring, L. M. (1997). Hydraulic fracture with multiple segments I. Observations and model formulation. International Journal of Rock Mechanics and Mining Sciences, 34(3-4), 97-e1.

Germanovich, L. N., and Dyskin, A. V. (2000). Fracture mechanisms and instability of openings in compression. International Journal of Rock Mechanics and Mining Sciences, 37(1), 263-284.

Groenenboom, J., and van Dam, D. B. (2000). Monitoring hydraulic fracture growth: Laboratory experiments. Geophysics, 65(2), 603-611.

Guilbaud, S., and Audoin, B. (1999). Measurement of the stiffness coefficients of a viscoelastic composite material with laser-generated and detected ultrasound. The Journal of the Acoustical Society of America, 105(4), 2226-2235.

Hallam, S. D., and Last, N. C. (1991). Geometry of hydraulic fractures from modestly deviated wellbores. Journal of Petroleum Technology, 43(06), 742-748.

Hanson, M. E., Anderson, G. D., Shaffer, R. J., and Thorson, L. D. (1982). Some effects of stress, friction, and fluid flow on hydraulic fracturing. Society of Petroleum Engineers Journal, 22(03), 321-332.

Hornby, B. E. (1998). Experimental laboratory determination of the dynamic elastic properties of wet, drained shales. Journal of Geophysical Research: Solid Earth, 103(B12), 29945-29964.

Hubbert, M. K., and D. G. Willis (1957). Mechanics of hydraulic fracturing, Journal of Petroleum Technology, 9, 153 – 166.

Hull, D. (1994). The evolution of ‘cone’ cracks under axi-symmetric loading conditions. International journal of fracture, 66(4), 295-312.

Hull, D. (1994). The effect of mixed mode I/III on crack

evolution in brittle solids. International journal of fracture, 70(1), 59-79.

Jacquot, P., and J. M. Fournier (2000). Interferometry in speckle light: Theory and applications: Springer.

James Verdon (2012). SEIS_PICK: An interactive seismic picking environment for MATLAB, University of Bristol, BUMPS (Bristol University Microseismicity ProjectS)

Jech, J. (1991). Computation of elastic parameters of anisotropic medium from travel times of quasi-compressional waves. Physics of the Earth and Planetary Interiors, 66(3-4), 153-159.

Jeffrey, R. G., and Settari, A. (1995, January). A comparison of hydraulic fracture field experiments, including mineback geometry data, with numerical fracture model simulations. In SPE Annual Technical Conference and Exhibition. Society of Petroleum Engineers.

Johnson, E., and Cleary, M. P. (1991, January). Implications of recent laboratory experimental results for hydraulic fractures. In Low Permeability Reservoirs Symposium. Society of Petroleum Engineers.

Kanninen, M.F., and C.H. Popelar (1985). Advanced Fracture Mechanics, Oxford University Press, New Yok, 563 pp.

Knauss, W. G. (1970). An observation of crack propagation in anti-plane shear. International Journal of Fracture, 6(2), 183-187.

Lebedev, M., Bóna, A., Pevzner, R., and Gurevich, B. (2011). Elastic anisotropy estimation from laboratory measurements of velocity and polarization of quasi-P-waves using laser interferometry. Geophysics, 76(3), WA83-WA89.

Lecampion, B., and Peirce, A. (2007). Multipole moment decomposition for imaging hydraulic fractures from remote elastostatic data. Inverse problems, 23(4), 1641.

Liao, J. J., Hu, T. B., and Chang, C. W. (1997). Determination of dynamic elastic constants of transversely isotropic rocks using a single cylindrical specimen. International Journal of Rock Mechanics and Mining Sciences, 34(7), 1045-1054.

Lo, T. W., Coyner, K. B., and Toksöz, M. N. (1986). Experimental determination of elastic anisotropy of Berea sandstone, Chicopee shale, and Chelmsford granite. Geophysics, 51(1), 164-171.

Martin, D., Pouet, B., and Rasolofosaon, P. N. J. (1994). Laser ultrasonics applied to seismic physical modeling. Seismic physical modeling: SEG Geophysics Reprint Series, 15, 499-511.

Medlin, W. L., and Masse, L. (1984). Laboratory experiments in fracture propagation. Society of Petroleum Engineers Journal, 24(03), 256-268.

Monchalin, J. P. (1986). Optical detection of ultrasound. IEEE Transactions on Ultrasonics Ferroelectrics and Frequency Control, 33, 485-499.

Monchalin, J. P., Aussel, J. D., Héon, R., Jen, C. K., Boudreault, A., and Bernier, R. (1989). Measurement of in-plane and out-of-plane ultrasonic displacements by optical heterodyne interferometry. Journal of Nondestructive Evaluation, 8(2), 121-133.

Nishizawa, O., Satoh, T., Lei, X., and Kuwahara, Y. (1997). Laboratory studies of seismic wave propagation in inhomogeneous media using a laser Doppler vibrometer. Bulletin of the Seismological Society of America, 87(4), 809-823.

Nordgren, R. P. (1972). Propagation of a vertical hydraulic fracture. Society of Petroleum Engineers Journal, 12(04), 306-314.

Ogi, H., Nakamura, N., Sato, K., Hirao, M., and Uda, S. (2003). Elastic, anelastic, and piezoelectric coefficients of langasite: Resonance ultrasound spectroscopy with laser-Doppler interferometry. IEEE transactions on ultrasonics, ferroelectrics, and frequency control, 50(5), 553-560.

Ong, O. N., Schmitt, D. R., Kofman, R. S., and Haug, K. (2016). Static and dynamic pressure sensitivity anisotropy of a calcareous shale. Geophysical Prospecting, 64(4), 875-897.

Perkins, T. K., and Kern, L. R. (1961). Widths of hydraulic fractures. Journal of Petroleum Technology, 13(09), 937-949.

Pollard, D. D., and Aydin, A. (1988). Progress in understanding jointing over the past century. Geological Society of America Bulletin, 100(8), 1181-1204.

Pollard, D. D., Segall, P. A. U. L., and Delaney, P. T. (1982). Formation and interpretation of dilatant echelon cracks. Geological Society of America Bulletin, 93(12), 1291-1303.

Pouet, B., and Rmolofosaon, P. N. (1990). Seismic physical modeling using laser ultrasonics. In SEG Technical Program Expanded Abstracts 1990 (pp. 841-844). Society of Exploration Geophysicists.

Pouet, B. F., and Rasolofosaon, N. J. P. (1993). Measurement of broadband intrinsic ultrasonic attenuation and dispersion in solids with laser techniques. The Journal of the Acoustical Society of America, 93(3), 1286-1292.

Pros, Z., and Babuška, V. (1967). A method for investigating the elastic anisotropy on spherical rock samples. Zeitschrift für Geophysik, 33(4), 289-291.

Rasolofosaon, P. N., and Zinszner, B. E. (2002). Comparison between permeability anisotropy and elasticity anisotropy of reservoir rocks. Geophysics,

67(1), 230-240.

Rasolofosaon, P. N., Martin, D., Rasolofosaon, P. N. J., Gascón, F., Bayón, A., and Varadé, A. (1994). Physical modeling of 3D seismic wave propagation. In Modeling the Earth for Oil Exploration (pp. 637-686).

Roering, C. (1968). The geometrical significance of natural en-echelon crack-arrays. Tectonophysics, 5(2), 107-123.

Rittel, D. (2000). Experimental investigation of transient thermoplastic effects in dynamic fracture. International journal of solids and structures, 37(21), 2901-2913.

Rummel, F. (1987). Fracture mechanics approach to hydraulic fracturing stress measurements. Fracture mechanics of rock, 217.

Sahouryeh, E., Dyskin, A. V., and Germanovich, L. N. (2002). Crack growth under biaxial compression. Engineering Fracture Mechanics, 69(18), 2187-2198.

Sarout, J., Molez, L., Guéguen, Y., and Hoteit, N. (2007). Shale dynamic properties and anisotropy under triaxial loading: Experimental and theoretical investigations. Physics and Chemistry of the Earth, Parts A/B/C, 32(8), 896-906.

Scruby, C. B., and Drain, L. E. (1990). Laser ultrasonics techniques and applications. CRC Press.

Siggins, A. F., and Dewhurst, D. N. (2007). Ultrasonic determination of the elastic constants of VTI shale. In Proceedings of the International Congress on Ultrasonics.

Sommer, E. (1969). Formation of fracture 'lances' in glass. Engineering Fracture Mechanics, 1(3), 539IN11541-540IN14546.

Takada, A. (1990). Experimental study on propagation of liquid filled crack in gelatin: Shape and velocity in hydrostatic stress condition. Journal of Geophysical Research: Solid Earth, 95(B6), 8471-8481.

Thomsen, L. (1986). Weak elastic anisotropy. Geophysics, 51(10), 1954-1966.

Vestrum, R. W. (1994). Group and phase-velocity inversions for the general anisotropic stiffness tensor. Geology and Geophysics, University of Calgary.

Warpinski, N. R., Clark, J. A., Schmidt, R. A., and Huddle, C. W. (1982). Laboratory investigation on the-effect of in-situ stresses on hydraulic fracture containment. Society of Petroleum Engineers Journal, 22(03), 333-340.

Warpinski, N. R., Schmidt, R. A., and Northrop, D. A. (1982). In-situ stresses: the predominant influence on hydraulic fracture containment. Journal of Petroleum Technology, 34(03), 653-664.

Warpinski, N. R. (1985). Measurement of width and pressure in a propagating hydraulic fracture. Society of Petroleum Engineers Journal, 25(01), 46-54.

Weijers, L., De Pater, C. J., Owens, K. A., and Kogsbøll, H. H. (1994). Geometry of hydraulic fractures induced from horizontal wellbores. SPE Production and Facilities, 9(02), 87-92.

Wu, R., Germanovich, L. N., Van Dyke, P. E., and Lowell, R. P. (2007). Thermal technique for controlling hydraulic fractures. Journal of Geophysical Research: Solid Earth, 112(B5).

Yukio, U., Kazuo, I., Tetsuya, Y., and Mitsuru, A. (1983). Characteristics of brittle fracture under general combined modes including those under bi-axial tensile loads. Engineering Fracture Mechanics, 18(6), 1131-1158.

Zhou, J., Chen, M., Jin, Y., and Zhang, G. Q. (2008). Analysis of fracture propagation behavior and fracture geometry using a tri-axial fracturing system in naturally fractured reservoirs. International Journal of Rock Mechanics and Mining Sciences, 45(7), 1143-1152.

*CORRESPONDING AUTHOR: Rajesh R. NAIR,
Petroleum Engineering, Petroleum Geomechanics Laboratory,
Department of Ocean Engineering, Indian Institute of Technology Madras,
Chennai, Tamil Nadu,
India
email: rajeshnair@iitm.ac.in